Effects of Uniaxial Drawing and Heat-Treatment on Gas Sorption and Transport in PVC

M. J. EL-HIBRI and D. R. PAUL, *Department of Chemical Engineering and Center for Polymer Research, University of Texas, Austin, Texas 78712*

Synopsis

Sorption and transport measurements for various gases in rigid poly(vinyl chloride) were made following uniaxial drawing and heat treatment. The permeabilities of He, Ar, N_2, and CH_4 were found to be essentially independent of pressure in PVC while CO_2 showed a complex pressure dependence which varied with prior exposure and degassing history. Sorption isotherms were analyzed by the dual mode sorption model, and the parameters obtained were correlated with the Lennard–Jones potential-well depth of the gas. The Henry's law coefficient for CO_2 was found to be significantly larger than expected which is believed to be the result of a specific interaction with PVC. Uniaxial drawing of PVC above its glass transition caused significant reductions in gas permeabilities, of which roughly one-third is attributable to the accompanying heat treatment rather than molecular orientation per se. The physical state of the polymer was characterized by density, birefringence, and calorimetry. Changes in gas sorption and permeation behavior are discussed in terms of these results.

INTRODUCTION

Fabrication and forming of polymeric products frequently involves a series of thermal and mechanical treatments which inevitably affect the final physical properties of the polymer. Apart from crystallinity, molecular orientation is one of the most important physical structural features of a polymer.

The effects of molecular orientation on gas transport in polymers often involve the simultaneous interplay of several variables, e.g., crystallinity, amorphous orientation, crystalline orientation, etc., which makes it difficult to assess each individual contribution separately. In the early studies on oriented semicrystalline polymers, changes in gas sorption and transport have routinely been interpreted in terms of changes in crystallinity and/or crystalline orientation without concern about orientation in the amorphous phase.[1-4] However, over the past 15 years interest in amorphous orientation has grown steadily as indicated by the work of Brady and coworkers,[5] Barker et al.,[6] and most recently Porter and Wang.[7]

In view of the importance of orientation processes on transport behavior and the relatively sparse literature on the subject, we were prompted to initiate a series of studies in this area of which this first paper is devoted to poly(vinyl chloride). Our studies differ from most of the past work in several regards. First, it is recognized that gas permeation is the resultant of solubility and mobility phenomena, and either or both may be affected by orientation processes. Second, it is recognized that, to introduce molecular orientation in a polymer, the material is typically drawn above its

Journal of Applied Polymer Science, Vol. 30, 3649–3678 (1985)
 CCC 0021-8995/85/093649-30$04.00

glass transition temperature. Thus, the drawing process is almost invariably comprised of a thermal treatment in addition to molecular orientation. Therefore, in order to assess accurately the effects of orientation, the changes caused by the thermal treatment must also be determined. Most studies on molecular orientation to date have not devoted adequate attention to this issue. Also, knowledge of the extent of molecular orientation (such as draw ratio or an orientation function) alone is not sufficient for predicting the gas transport behavior of the material without knowledge of the *conditions* under which orientation was performed. The most important such processing variable is the drawing temperature. This study was designed while taking the above factors into account.

Only uniaxial orientation effects have been considered here. Biaxial orientation, having been partly examined, appears to affect gas transport in ways that differ fundamentally from those of the uniaxial case. Therefore, the results of this study must not be generalized to the biaxial case.

EXPERIMENTAL

Materials

Two PVC films were used in this study. The first was a 1.5 mil experimental film prepared by B. F. Goodrich which contained no additives except for 2% of a tin stabilizer.[8] This film was used to characterize the gas sorption, transport and physical properties of rigid PVC and to serve as a reference material against which to check the other film used. The latter was a commercial product made by Klochner Pentaplast of America designated as Pentaform Type TH 170/01 which contained approximately 3 parts per hundred of an acrylic impact modifier. This film had excellent surface quality and thickness uniformity (nominally 5 mils) and was used for all oriented and annealed sample preparations. Table I lists some physical and mechanical properties for the two materials along with literature values.[9] Neither material showed any evidence by thermal analysis of an endotherm characteristic of ordinary primary crystallinity in the melting region known for semicrystalline PVC. However, a broad shallow curvature in DSC thermograms does appear above ~110°C and is believed to be associated with the existence of roughly 5–10% imperfect crystalline order that is generally known to be present in commercial PVC.

The gases used for sorption and transport measurements were He, Ar, N_2, CH_4, and CO_2. The purity of all gases was 99.7% or better except for CH_4, which was 99.0%.

Sample Preparation

A Table Model Instron fitted with an environmental chamber was used to prepare all the uniaxially drawn and annealed samples. The chamber was lined with insulation and contained heating elements, covered with aluminum foil to reduce radiation effects, and coupled to a power regulator and a temperature controller. Blowers were placed inside the chamber for internal circulation, and another, on the outside, provided forced air for

TABLE I
Physical and Mechanical Properties for PVC Films Used

Film	CS 5760	Pentaform TH 170/01	Literature values[a]
Source	B. F. Goodrich	Klockner Pentaplast	—
Nominal thickness	1.5 mil	5 mil	—
Glass transition	71°C	75°C	70–87°C
Specific gravity	1.389	1.367	1.35–1.45
Refractive index	1.544	1.539	1.52–1.55
Yield (psi)	7.99×10^3	8.08×10^3	$5–9 \times 10^3$
Modulus (psi)	3.05×10^5	2.68×10^5	$3.5–6 \times 10^5$
Percent elongation at break	107	135	2–40

[a] From ref. 9.

rapid cooling of the samples once the drawing or annealing was completed. Temperature control and uniformity were within ± 0.5°C.

Samples were prepared by first cutting 4.5 × 6 in. rectangular strips of film along the original machine direction of the as-received film on which parallel lines 2 in. apart were drawn in ink along the transverse direction of the film. The film was then clamped at both ends by two pairs of wide T-shaped aluminum grips using small C-clamps. This assembly was mounted onto the crosshead mechanism of the Instron inside the chamber, which was heated beforehand to the desired drawing temperature. Transient reheating time to the drawing temperature was about 5 min. Following that, the sample was maintained at the working temperature for exactly 15 min. This was done whether the sample was drawn or just heat-treated. In the case of oriented samples, drawing was performed at the end of the heating period, e.g., 13 min heating followed by 2 min drawing. This procedure insured that samples of different draw ratios and the undrawn samples experienced an identical heat history so that the effects of orientation can be isolated from those of thermal treatment alone. Drawing at or above 75°C was done with a crosshead speed of 2 in./min (100% min), whereas, below 75°C, a slower strain rate of 0.5 in./min (25%/min) was required to prevent premature breakage of the films.

After drawing or annealing, each sample was air-quenched to room temperature by the external blower at a cooling rate of about 50°C/min. The draw ratio was determined by dividing the final distance between the ink lines by the initial distance of 2.0 in. In the case of drawing above T_g, deformation occurred uniformly throughout the sample and, thus, the nominal draw ratio defined above was also the actual draw ratio; for the sub-T_g drawing, however, this apparent draw ratio was somewhat lower than the actual draw ratio because of the necking mechanism of deformation. The actual draw ratios were obtained by following additional ink lines drawn in the central region of the undrawn specimen. The reported draw ratios are actual and not nominal values.

Samples for sorption or permeation measurements were taken from the central section of oriented specimens to insure consistency in the compar-

isons of various samples and because only the central part of the drawn film satisfied the condition of truly uniaxial orientation.

Sorption and Transport Measurement

The gas sorption measurements were carried out at 35°C using a dual-volume, dual-transducer cell design based on the pressure decay principle. Details about the components and operation of this device have been reported previously.[10,11] The only modification to the procedures described earlier is that in the case of N_2, Ar, and CH_4 sorption, where solubility coefficients are very small, an increase in the sample volume from the usual 2 cm^3 to about double that amount brought about marked improvements in the acquisition and accuracy of the sorption isotherm data.

The equipment and procedures for the permeation measurements have also been described earlier.[10,12] The all-metal construction of the permeation cell allows gas transport measurements at pressures up to 30 atm. Time lag and permeability values were obtained by continuously monitoring the pressure rise downstream from the membrane. Very accurate thickness determinations for the samples were obtained by calculations based on the known membrane area, weight, and density and by a micrometer. Agreement between the two methods was excellent, and the thickness values used in calculations were always accurate to ± 0.5 μm.

The permeability and time-lag measurements for Ar and N_2 on all the commercial Klockner films were done at a 20 atm upstream driving pressure. Since permeabilities for Ar and N_2 are of the order of 10^{-12} and 10^{-13} [cm^3(STP) cm/cm^2 s cm Hg], it was necessary to achieve permeation rates high enough to render air leakage rates into the system insignificant. For He, a constant pressure of 3 atm was employed throughout. The level of accuracy and reproducibility for the transport data was within $\pm 1.5\%$ of the reported values for P and about $\pm 3\%$ for apparent diffusion and solubility coefficients. For sorption isotherms, a remarkable reproducibility of better than ± 0.02 cm^3(STP)/cm^3 was obtained for N_2, Ar, and CH_4 by doubling the sample size as indicated above. This was better than the precision level associated with the much more sorptive gas CO_2.

Physical Characterization

PVC density measurements were performed at 30°C in a density gradient column using aqueous solutions of calcium nitrate. Glass floats, factory-calibrated to ± 0.0001 g/cm^3, were used to calibrate the liquid gradient. Density measurements were accurate within ± 0.0002 g/cm^3.

Birefringence Δ was used to characterize the state of orientation in uniaxially drawn PVC. The measurements were performed using a Babinet compensator with accuracy of $\pm 0.05 \times 10^{-3}$.

Thermal analysis of as-received, annealed and oriented PVC samples was performed on a Perkin-Elmer DSC-2 differential scanning calorimeter interfaced to a computerized control and data acquisition system. A scanning rate of 20°C/min was used in all cases. Sample weights were 15–18 mg, but all reported DSC results were normalized to a unit mass basis for comparison purposes.

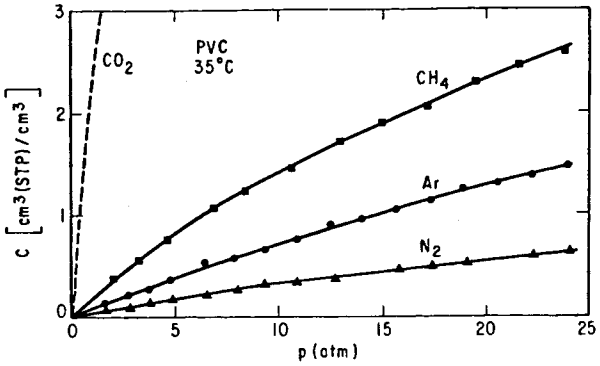

Fig. 1. Sorption isotherms for N_2, Ar, and CH_4 in PVC at 35°C.

GAS SORPTION AND TRANSPORT IN UNTREATED PVC

Sorption

Figures 1 and 2 show sorption isotherms for N_2, Ar, CH_4, and CO_2 at 35°C for the "as-received" B. F. Goodrich film. The solubilities for the Klockner sample did not differ significantly as Figure 21 shows for CO_2. All of the isotherms are well described by the dual sorption model

$$C = k_D p + \frac{C'_H b p}{1 + bp} \tag{1}$$

Interpretations of the physical significance of the model and each of the parameters k_D, C'_H, and b have been presented elsewhere.[13,14] Table II shows the sorption parameters for N_2, Ar, CH_4, and CO_2 at 35°C computed using a least-squares fitting algorithm. The sorption data and parameters presented here are the most extensive to be published for PVC to date. Berens[15] reported low-pressure sorption data for N_2 and CO_2 in PVC and estimated the dual mode parameters for the latter. Our k_D value for CO_2 agrees reasonably well with Berens' value of 0.7 cc(STP)/cc atm, but C'_H and b are substantially different, largely due to the narrow pressure range used in Berens' study, which precludes accurate estimates for these parameters.

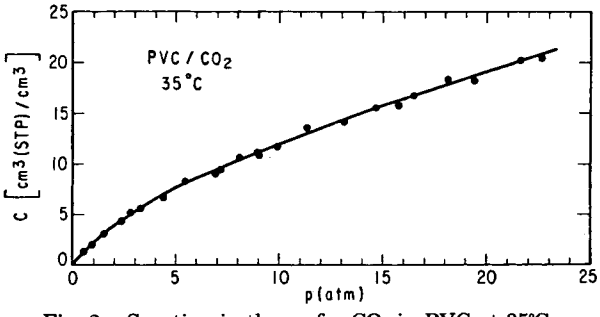

Fig. 2. Sorption isotherm for CO_2 in PVC at 35°C.

TABLE II
PVC Sorption Parameters for Various Gases at 35°C

Gas	ϵ/k (K^{-1})	k_D [cm^3(STP)/cm^3 atm]	C'_H [cm^3(STP)/cm^3]	b (atm^{-1})	$k_D + C'_D b$	k_a
N_2	91.5	0.0169	0.4505	0.0448	0.0371	0.0341
Ar	124	0.0377	1.132	0.0410	0.0841	0.0800
CH_4	137	0.0513	2.305	0.0622	0.1946	0.2160
CO_2	190	0.587	8.939	0.2094	2.458	0.9644

The sorption extents for the various gases follow the ascending order of N_2 < Ar < CH_4 < CO_2 as observed for all the other glassy polymers studied so far. The sorption data expressed in terms of the dual sorption model can be roughly correlated by plotting the logarithm of the sorption parameters against the Lennard–Jones potential parameter ϵ/k for the gas,[16] as shown in Figures 3–6. The approximate linearity of the relationships has been established in previous studies.[13,17–19] In Figure 3 the straight line for log k_D vs. ϵ/k was drawn using the N_2, Ar, and CH_4 points only. The observed k_D value for CO_2 was about three times larger than the value expected based on the straight line correlation. This abnormally large CO_2 solubility may result from favorable polar interactions between the CO_2 and the PVC repeat unit, which are not present for the other gases. Similar, unexpectedly high CO_2 solubilities relative to other gases (e.g., CH_4) have been reported recently by Koros[20] for cellulose acetate and PMMA. Those results have also been attributed to a specific gas/polymer interaction effect. In the

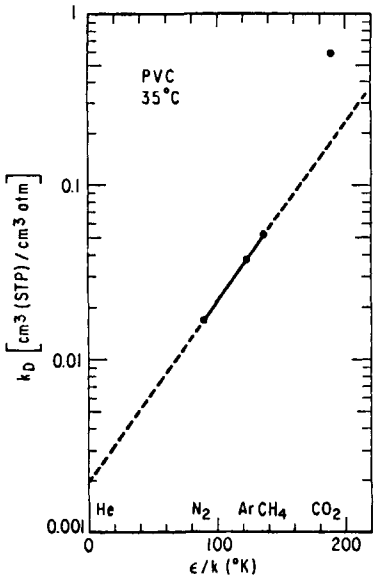

Fig. 3. Henry's law constant k_D vs. the Lennard–Jones parameter ϵ/k (CO_2 point was not included in fitting the straight line).

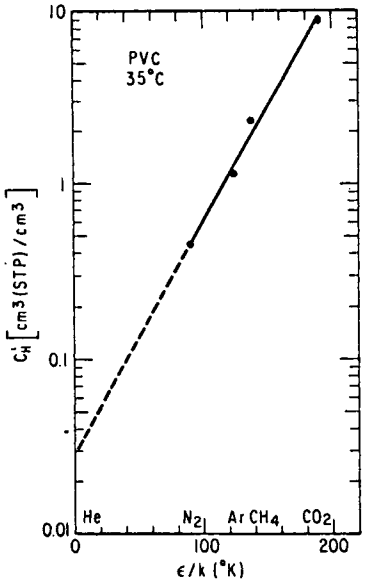

Fig. 4. Hole saturation constant C'_H vs. the Lennard–Jones parameter ϵ/k.

absence of specific gas/polymer interactions, plots of log k_D vs. ϵ/k generally yield straight lines with essentially the same slope (0.96×10^{-2} K^{-1}) for all polymers regardless of state (glassy or rubbery).[17] The slope of the line in Figure 3 is 1.06×10^{-2} K^{-1} in reasonable agreement with other polymers and, thus, reinforces the notion that the CO_2 value is unusually large. A similar deviation from the linear line was not observed for CO_2 in the correlations involving C'_H and b, shown in Figures 4 and 5, respectively. This finding is important in that it further illustrates a fundamental distinction between the ordinary (Henry's law) and Langmuir gas dissolution modes.

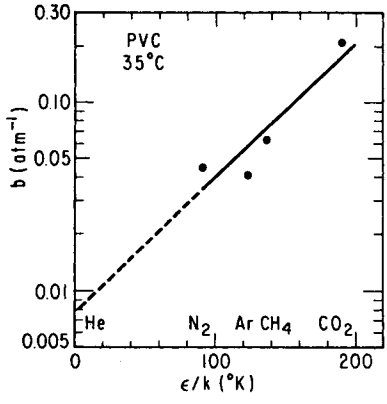

Fig. 5. Hole affinity constant b vs. the Lennard–Jones parameter ϵ/k.

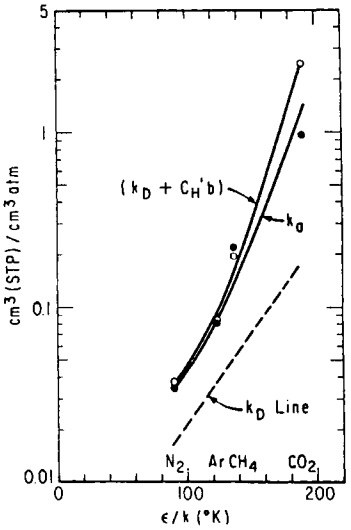

Fig. 6. Apparent Henry's law coefficient measured by the equilibrium and transient methods vs. ϵ/k: (○) $(k_D + C'_Hb)$ from sorption; (●) k_a from transport. $p_2 \sim 1 - 2$ atm.

Figure 6 compares the initial slope of the sorption isotherm, $k_D + C'_Hb$, with the apparent gas solubility coefficient, k_a, computed from transient permeation measurements at low driving pressures, i.e., $k_a = P/D_a$, where the apparent diffusion coefficient is related to thickness and time lag by

$$D_a = l^2/6\theta \tag{2}$$

Based on the correlations seen in Figures 3–5, straight lines are not expected in Figure 6. The two measures of apparent solubility agree well (see Table II also) except in the case of CO_2.

Transport

Gas permeation in glassy polymers has frequently been analyzed using a dual mobility model,[21] which envisions the existence of two distinct diffusion coefficients, D_D and D_H, associated with the two modes of sorption. This model leads to the following expression for the permeability coefficient:

$$P = k_D D_D \left(1 + \frac{FK}{1 + bp_2}\right) \tag{3}$$

where p_2 is the upstream driving pressure, $F = D_H/D_D$, and $K = C'_Hb/k_D$. In general, this expression suggests that P should be a mildly decreasing function of p_2 as observed for a variety of glassy polymers.[13,15–17]

Permeability data for He, Ar, N_2, and CH_4 in the B. F. Goodrich PVC are shown in Figure 7 as a function of upstream pressure. For the first three gases, there is no dependence of P on pressure implying the special case of

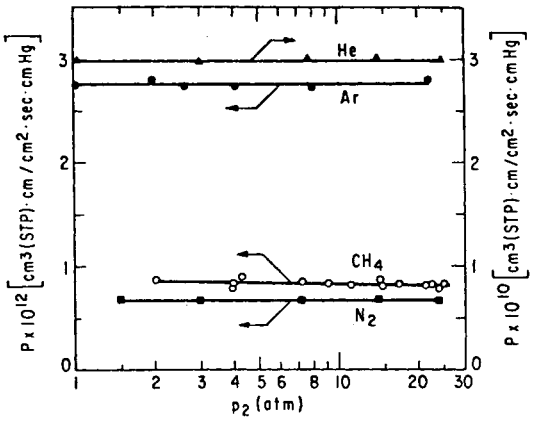

Fig. 7. Permeability of various gases in PVC at 35°C vs. the upstream driving pressure p_2.

"total immobilization" of the Langmuir mode or $F = 0$ in terms of the model embodied in Eq. (3). On the other hand, methane exhibits a small decline, about 5%, in P over this pressure range, but the CH_4 data also exhibit more scatter than the data for the other three gases. In Table III, permeabilities and apparent diffusion coefficients for the various gases in the two PVCs are tabulated along with values extracted by interpolation from the data of Tikhomirov et al.,[22] which is the only extensive source in the literature reporting on the transport of various gases in unplasticized PVC. Our data agree quite well with the reported values for He and Ar, but diverge greatly for the other gases, particularly N_2 and CH_4. Roberts and Kammermeyer[23] have also reported some results for He, CH_4, and CO_2, but their P values are another order of magnitude larger than Tikhomirov's values. Our results follow reasonable trends while the Tikhomirov data contain some inconsistencies. For example, this reference gives nearly identical permeabilities for Ar and N_2 whereas, based on the behavior of other polymers, one expects N_2 to always have both a lower solubility and lower

TABLE III
Permeability[a] and Apparent Diffusion Coefficients of Various Gases in Two PVCs at 35°C along with Values Interpolated from the Data of Tikhomirov et al.[22]

	P [cm³(STP)cm/cm² s cm Hg]			D_a (cm²/s)		
Gas	Pentaform	CS5760	Tikhomirov	Pentaform	CS5760	Tikhomirov
He	3.36×10^{-10}	2.98×10^{-10}	3.1×10^{-10}	—	—	4.0×10^{-6}
Ar	3.69×10^{-12}	2.77×10^{-12}	2.7×10^{-12}	3.39×10^{-9}	2.42×10^{-9}	2.3×10^{-9}
N_2	9.45×10^{-13}	6.68×10^{-13}	2.8×10^{-12}	1.88×10^{-9}	1.37×10^{-9}	8.0×10^{-9}
CH_4	1.08×10^{-12}	8.50×10^{-13}	6.0×10^{-12}	—	3.31×10^{-10}	3.1×10^{-9}
CO_2	2.43×10^{-11}	1.84×10^{-11}	3.2×10^{-11}	1.45×10^{-9}	1.45×10^{-9}	5.5×10^{-9}

[a] Upstream pressures for He, Ar, N_2, and CH_4 measurements of P and D_a were 20 atm for the Pentaform film and 0.5–2.0 atm for the other two materials. For CO_2 an upstream pressure of ~1.0 atm was used for all three materials.

diffusion coefficient than Ar. The diffusion coefficient for CH_4 given in the Tikhomirov paper is larger than that of Ar (see Table III), which is not physically realistic since the molecular diameter of CH_4 is larger than that for Ar. The P and D_a values for the commercial Klockner product are somewhat larger than those for the B. F. Goodrich film due to the impact modifier and possibly to differences in the thermal histories of the two samples. Figure 8 shows time lag data for CH_4, N_2, and Ar in the experimental PVC film as a function of upstream driving pressure. As expected, CH_4 shows a stronger decrease in θ with p_2 than do N_2 or Ar.

The permeation of CO_2 in PVC is a complex function of prior history as demonstrated in Figure 9. The curve labeled "1" represents an initial sequence of runs made on as-received film by sequentially increasing the pressure from 1 atm to about 25 atm, allowing adequate time at each pressure to reach an apparent steady-state. For high pressure, this took much longer than the usual four to five time lags which proved sufficient for the other gases. For the 25 atm measurement, the pressure was held for 24 h, after which the film was degassed for 35 h or about 90 time lags. A second sequence of measurements were made on the same film again beginning at 1 atm and progressing sequentially to higher pressures. As seen in Figure 9, this gave significantly higher permeabilities, especially at low pressures, than did the first sequence. After this, the sample was removed from the permeation cell and then reinstalled after one week. After degassing for 24 h, the third sequence of measurements were made in the same manner as the first two. Finally, after the maximum pressure of 25 atm was reached, the pressure was varied randomly up and down the pressure scale without evacuation between runs, giving curve 4 in Figure 9. Each run lasted until no change in flux occurred over at least 10 h, and the so-obtained permeabilities are essentially independent of pressure as seen for the other gases. This complex behavior is a consequence of a rather significant plasticizing influence of CO_2, which alters the state of glassy polymers even after the CO_2 is removed. Such "conditioning" effects have been observed before[19,24,25] for other glassy polymers; however, PVC appears

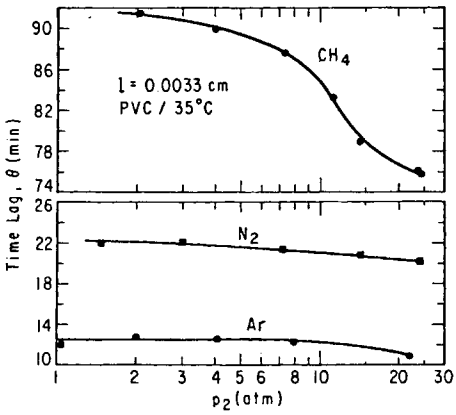

Fig. 8. Time lag vs. the upstream driving pressure p_2, for Ar, N_2, and CH_4 in PVC at 35°C.

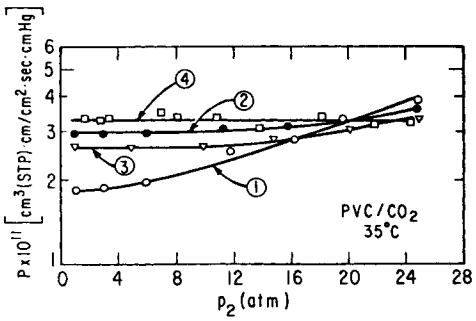

Fig. 9. Permeability of CO_2 in PVC at 35°C as a function of upstream driving pressure p_2. Runs were made in four sequences, in ascending pressure order: (○); 1st sequence; (●) 2nd sequence after 36 h evacuation; (▽) 3rd sequence after 1 week evacuation; (□) 4th sequence with no evacuation from 3rd sequence.

to be different in that the changes in state occur over longer time periods and may be less stable once established than those observed for other glassy polymers. The strong influence of CO_2 on PVC is made clear by the observation that sorption of CO_2 at 25 atm lowers the T_g by about 25°C as described elsewhere.[26] Owing to the severe time dependence of the CO_2 conditioning on PVC permeation characteristics, care must be exercised in attempts to interpret the effect of pressure on permeability. For example, curves 1–3 in Figure 9 might be regarded to be in accord with various models which predict P to *increase* with p_2[27,28] whereas, in fact, upon more complete conditioning the permeability appears to be independent of pressure (curve 4). In this case, transport behavior is not just a function of CO_2 concentration or pressure, but also depends on long term relaxations at any given condition.

Time lag data for PVC in CO_2 is plotted as a function of pressure in Figure 10. The conditions under which these values were measured were very strictly controlled to obtain the most reproducible data possible. A 2-mil film different from the one used for P determinations was initially "vec-

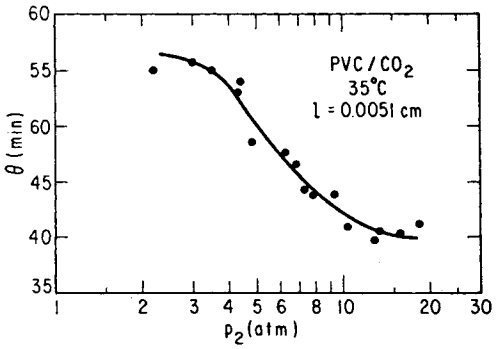

Fig. 10. Time lag data for CO_2 in PVC as a function of upstream driving pressure p_2 at 35°C. The sample was initially exposed to 20 atm CO_2 for 3 days on the upstream side. Evacuation time between runs was ~10 h.

tored" (i.e., exposed to CO_2 on the upstream side only) with 20 atm of CO_2 for 3 days. Before each run, the sample was evacuated 12–15 h, and the runs were carried to between 5 and 7 time lags at each pressure. The pressure sequence used for the runs was based on random selection. Over the pressure range from 2 to 20 atm, the time lag decreased by 30%. The corresponding time lag reductions for CH_4, N_2, and Ar were 16% for CH_4 and 10% for N_2 and Ar.

EFFECTS OF ANNEALING AND ORIENTATION

The following describes the effects of various treatments on properties of PVC. As mentioned earlier, certain annealing or heat treatment effects accompany any response caused by the drawing operation. To isolate this effect from orientation, some samples were given the same heat treatment but were not drawn, and they are referred to as having a draw ratio λ of 1.0 or by the notation 1.0X. Orientation of PVC was easiest to achieve at temperatures not far removed from T_g. In the range of temperatures from above 50 to 115°C, drawing could be performed with relative ease to 3.0X with 2.8X being the limit at 50°C. Thus, at $\lambda = 3.0$, the effect of drawing temperature was investigated. The maximum draw ratio possible under our operating conditions (~4.2X) was attainable at 100°C. This temperature was selected for study of the widest possible range of draw ratios on PVC properties.

The gases used to investigate the transport responses of PVC to various treatments were He, Ar, and N_2. Both CH_4 and CO_2 were excluded since CH_4 presented difficulty because of its very long time lags (~20 h for a 5 mil film) and CO_2 was avoided because of the complicated pressure and time dependence issues described earlier. For equilibrium sorption measurements, on the other hand, CO_2 is the only gas for which data are reported. It was difficult to discern differences in equilibrium sorption for Ar and N_2 since the changes induced were of the order of the accuracy limitations inherent in the sorption system so that apparent solubility behavior derived from transient permeation experiments was monitored instead.

Birefringence

The birefringence Δ of PVC drawn at 100°C is shown in Figure 11 as a function of draw ratio. The curve, characteristic of the pseudo-affine deformation mechanism,[29] is typical of many polymers drawn above T_g. The dependence of birefringence on the drawing temperature for fixed draw ratios is shown in Figure 12. The birefringence, and hence chain orientation, is markedly reduced as the drawing temperature is increased. A reduction of 65% is observed for a 2X-drawn sample over the temperature range from 55 to 125°C. The birefringence curves are continuous over the entire temperature range, i.e., no break at T_g, suggesting that the mechanism of chain alignment taking place both above and below T_g changes in a continuous manner. The birefringence plots of Figures 11 and 12 agree well with similar data for PVC from other sources, e.g., Hibi et al.[30] and Robinson and Bower.[31]

Exposure of oriented PVC film to high CO_2 pressures did not have a significant effect on the orientation state as Figure 13 illustrates for a

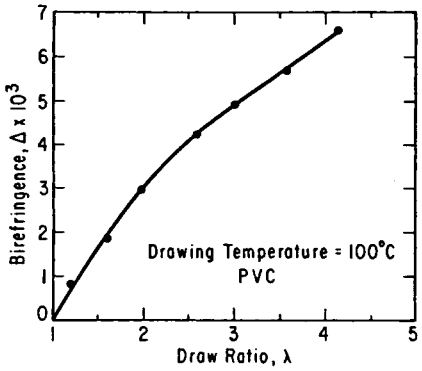

Fig. 11. Birefringence versus draw ratio for PVC drawn at 100°C.

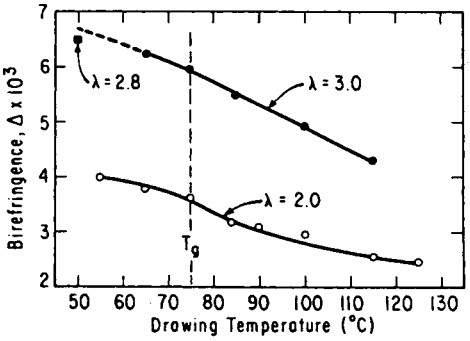

Fig. 12. Dependence of PVC birefringence on the drawing temperature at constant draw ratios of 2.0 and 3.0.

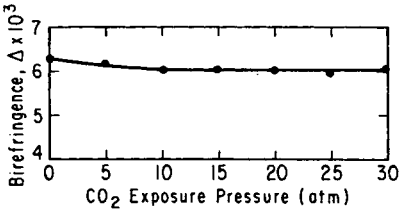

Fig. 13. Effect of CO_2 exposure at 35°C on the birefringence of oriented PVC ($\lambda = 4.1$). Exposure duration was 24 h at each pressure.

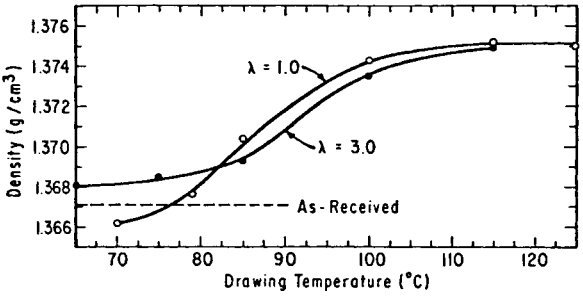

Fig. 14. Dependence of density for annealed ($\lambda = 1.0$) and drawn ($\lambda = 3.0$) PVC on the processing temperature.

sample drawn to 4.1X. The point at zero pressure represents the birefringence of the original sample before any exposure to CO_2. This sample was exposed to CO_2 at 35°C at successively higher pressures for 24 h each, and the birefringence was measured subsequent to every exposure. The approximate 5% drop in birefringence noted in Figure 13 may be due mainly to post-drawing relaxation at 35°C rather than to CO_2 exposure since CO_2 exposure is expected to be more effective at high pressures and not at pressures up to 10 atm where the decrease occurs.

Density

The effect of annealing and drawing on PVC density is shown in Figure 14 for a wide range of treatment temperatures. Heat treatment above T_g was predominantly responsible for all important density changes in PVC. Density increased with increasing annealing temperature and leveled off to an essentially constant value for temperatures $\geq$ 110°C. The "as-received" Klockner PVC is a calendered product that most probably had been quenched from high processing temperatures which explains its low density compared to heat-treated and drawn samples. It is not clear, however, why the density dips below the "as-received" value for the sample annealed at 70°C (below T_g). This reduction in density is also accompanied by an increase in argon diffusion coefficient as shown later.

The shape of the $\lambda = 3.0$ curve relative to that of $\lambda = 1.0$ is interesting. At drawing temperatures below T_g (up to 82°C) the density increases slightly relative to the "as-received" value as a result of drawing, while above 82°C drawing yielded lower density films compared to samples with the same thermal treatment but not drawn. Densification due to post-yield drawing below T_g has also been observed for polycarbonate.[32,33] Values of P and D_a are consistent with the observed increase in density with sub-T_g drawing. The air quenching procedure was applied uniformly to all the samples, but since the drawn samples were thinner than the annealed ones, they cooled somewhat faster. This may partly explain the slightly lower densities for the oriented samples in Figures 14 and 15. In Figure 15, the density of PVC is plotted as a function of draw ratio for a drawing temperature of 100°C.

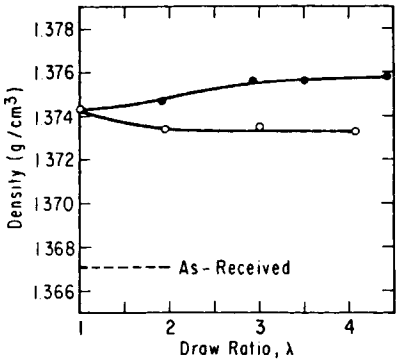

Fig. 15. PVC density as a function of draw ratio: (○) drawn at 100°C; (●) drawn at 100°C, then annealed (15 min).

The upper curve is for samples which were annealed under stress immediately following drawing. This annealing treatment was found to cause a slightly larger density at high draw ratios compared to samples which were simply drawn—see lower curve. It is apparent, therefore, that annealing above T_g and not orientation per se is mainly responsible for the densification of PVC.

The density results presented here cannot be compared directly with those reported by Brady et al.[5] since they did not make clear the effects that heat treatment had on the density. The results of the following calorimetric study give a clearer insight into the nature of physical changes occurring in PVC as a result of annealing and orientation.

Differential Scanning Calorimetry

The purpose of the calorimetric study was to determine whether the PVC samples used in this study were crystalline or not and to monitor any important physical changes occurring in the polymer due to the various processing steps. The scanning range for the thermograms reported here is from 17 to 227°C. The PVC melting point, estimated from Reding et al.'s study,[34] should be about 192°C for the material used in this work. For accurate comparison between the various DSC scans, all the thermograms were normalized to a 1 mg basis and accurate subtractions between endotherms were performed digitally by the computerized Thermal Analysis Data Station. All thermograms considered here are "first heats" following every particular treatment. DSC heats following the first were not of interest since the effects of sample history are erased during the course of the first heat; and, in fact, second heats looked essentially identical for all samples.

The effects of annealing at various temperatures above T_g ranging from 78 to 135°C are shown in the series of DSC scans presented in Figure 16 arranged in ascending order according to annealing temperature. The following features characterize the scans of Figure 16: (a) no melting endotherm near 192°C is associated with any of the annealed samples; (b) an

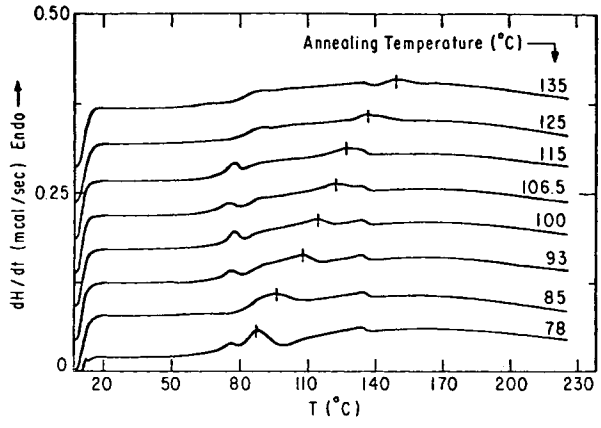

Fig. 16. DSC scans for samples annealed at various temperatures above T_g.

endothermic peak occurs near T_g which is about 75°C; (c) another endothermic peak occurs above T_g and shifts to higher temperatures as the annealing temperature is increased; and (d) a small endothermic "hump" of fixed size and position (135°C) also appears for all samples. The peak near T_g, which does not appear for all samples, is the result of different time spans between the sample preparation and DSC testing for different samples, i.e., room-temperature annealing. Not all the samples were prepared at the same time, and those samples which were exposed to ambient conditions for long periods developed the observed sub-T_g peak. Since the samples annealed at 85, 125, and 135°C were prepared only several hours prior to DSC testing they do not show any trace of such a peak. The second peak above T_g is a more interesting feature of the thermograms. This peak varies in both area and position as a function of the annealing temperature, and thus appears as a characteristic feature of annealing above T. The peak's position was always found to be 10–15°C above the annealing temperature, as shown in Figure 17. Such endothermic behavior for annealed PVC agrees well with the findings of several studies.[5,35-37] These peaks are suggestive of molecular order which is introduced into the polymer by annealing above T_g. This order is currently referred to in different ways. It is denoted by "secondary crystallinity," "mesomorphic order," or simply "molecular order." It is agreed upon among the various authors, however, that such regions possess a substantially lower degree of order than does conventional primary crystallinity. The order can be viewed to be arising from close packing of short chain segments especially those containing long sequences of syndiotactic dyads. Annealing above T_g has also been reported to increase the ratio of trans/gauche rotational isomers,[38] which would facilitate such an ordering process.

The area under the DSC annealing peak varies in an interesting manner. Since it was difficult to define the DSC endothermic area in an absolute manner, this area was defined by first subtracting the normalized DSC thermogram for the as-received sample from each of the annealed sample scans. The difference curve, which carried the annealing endotherm with it, was then analyzed. Figure 18 shows such a subtraction for a sample annealed at 115°C. The results of similar subtractions for annealing temperatures from 78 to 135°C are shown in Figure 19. The sub-T_g region subtraction was suppressed in these curves since it is irrelevant and would

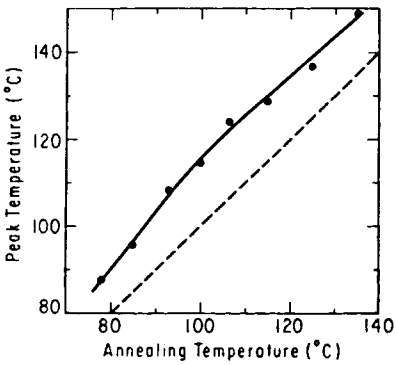

Fig. 17. DSC peak temperature for annealed PVC versus annealing temperature.

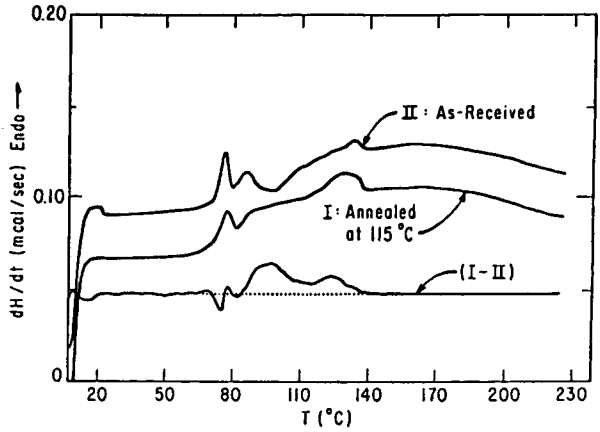

Fig. 18. DSC scans showing the effect of annealing at 115°C.

be confusing. Upon subtraction, a more subtle feature of these annealing endotherms appears in Figure 19 and that is the actual splitting of this endothermic region into two peaks, the first being fixed at 90°C whereas the second and smaller peak varies in position with annealing temperature as described earlier. The endothermic area was defined as the area between the DSC subtraction curve and the base line over the entire temperature range. This area was converted into cal/g to represent the "fusion" energy associated with the loss in order developed during annealing. It must be noted that only the second and smaller annealing peak changes in area and position with annealing temperature. Since this peak overlapped the 90°C peak at lower annealing temperatures and, thus, could not be separated from it, the entire area under the both peaks was analyzed. The calculated heats of fusion for the curves shown in Figure 19 are plotted against the annealing temperature in Figure 20. The dependence of ΔH on annealing temperature is quite interesting, exhibiting an increase up to the region of 100–110°C, where ΔH reaches a maximum and then begins to decline for

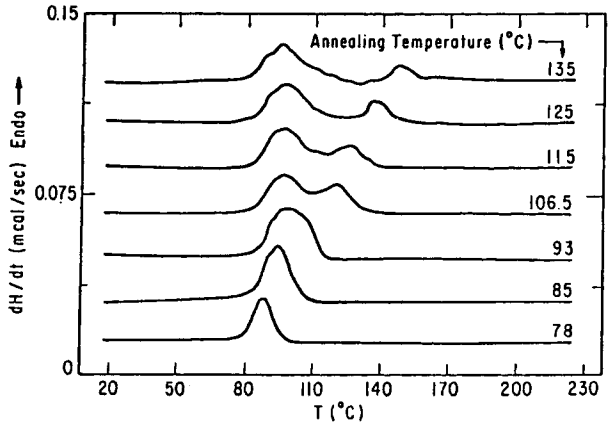

Fig. 19. DSC scans of PVC for various annealing temperatures after subtraction of "as-received" scan. (Sub-T_g events were suppressed from these curves for easier comparison.)

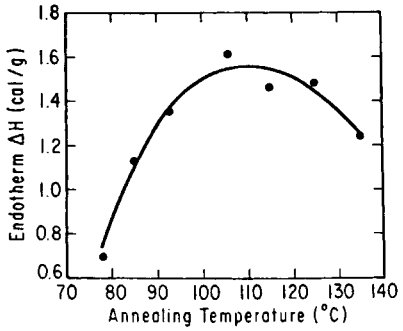

Fig. 20. Endotherm area versus annealing temperature for PVC.

higher annealing temperatures. This agrees well with the results of Brady et al.,[5] but differs from Brown et al.'s,[37] which places this maximum at 130°C. The shape of this curve is logical since ordering processes usually require an optimal segmental mobility or temperature that corresponds to the highest rate of ordering as in the case of crystallization.

Annealing PVC at temperatures below T_g did not induce any of the effects discussed above. Figure 21 shows how the net effect of sub-T_g annealing was to merely shift to a higher temperature the sub-T_g annealing peak, which is a very well-known phenomenon. The size and position of this peak are dependent on both annealing time and temperature. An extensive study on this topic has been done by Berens and Hodge.[39]

The effect of drawing PVC above the glass transition on the order introduced by annealing the polymer is quite unexpected. Figure 22 illustrates this effect by the subtraction of a 1.0X sample from a 4.2X sample subjected to the same heat treatment. The subtraction yields a substantially negative difference reflecting a strongly reduced order for the 4.2X sample relative to the undrawn but annealed sample. Evidently, the chain segments that form ordered bundles under annealing conditions are subjected to stress under drawing such that the bundle order is distorted. Furthermore, superimposed on this reduction in the annealing order is a lowering in the

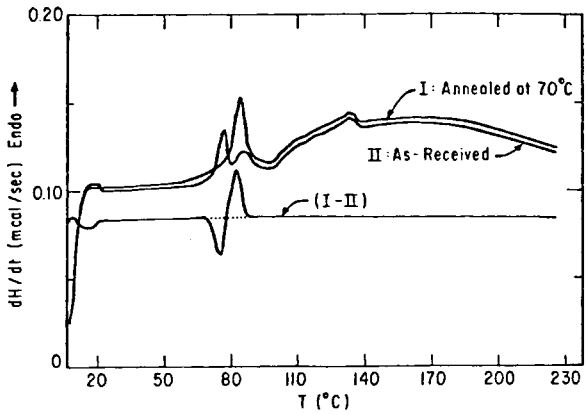

Fig. 21. DSC scans showing the effect of annealing at 70°C (sub-T_g).

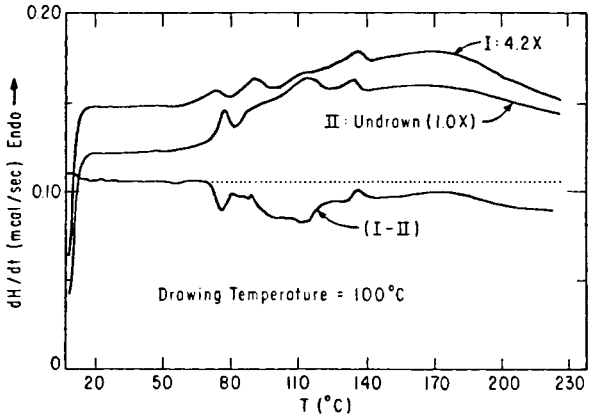

Fig. 22. DSC scans showing the effect of uniaxial drawing above T_g.

base line for the oriented sample in the region above T_g, suggesting a reduction in the heat capacity due to orientation. Orientation in amorphous polymers has been thought to cause reductions in the heat capacity and is known to reduce the thermal conductivity of the material.[39-41] The broad and shallow curvature that appears in the DSC baseline above ~110°C is probably indicative of some crystalline or mesomorphic order which is known for PVC, but this DSC curvature was almost identical for samples subjected to different annealing treatments as well as for the as-received film.

CO_2 Sorption

Since gas transport through polymers is the resultant of both sorption and diffusion, independent examination of the two processes is necessary. The sorption isotherms for CO_2 in PVC subjected to annealing and orientation at 85°C are shown in Figure 23 along with that of an "as-received" sample. Model parameters are given in Table IV. The extent of CO_2 sorption

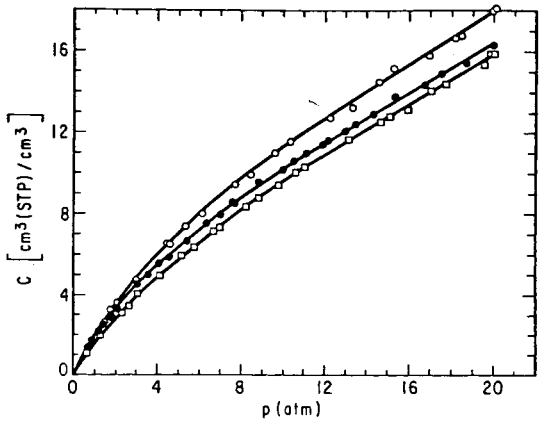

Fig. 23. CO_2 sorption isotherms at 35°C for PVC: (○) as received; (●) heated at 85°C (15 min); (□) drawn to 3.0X at 85°C.

TABLE IV
CO_2 Sorption Parameters at 35°C for PVC Subjected to Annealing and Orientation at 85°C

Sample	k_D	C'_H	b
"As received"	0.576	8.04	0.203
1X at 85°C	0.634	4.85	0.361
3X at 85°C	0.580	5.16	0.243

is reduced by the thermal treatment at 85°C and drawing to 3.0X in addition produces only a modest further reduction compared to the as-received material. Similar responses for Ar and N_2 were seen in the apparent solubility coefficients deduced from transport measurements.

Transport of He, Ar, and N_2

Permeabilities for He, Ar, and N_2 are plotted against the draw ratio in Figure 24. The relative permeability P/P_0 used to correlate the data is simply the ratio for a given gas of the permeability P for the treated material to the "as-received" permeability value P_0. Values for P_0 are tabulated in Table III under the Pentaform heading. The drawing temperature for all these samples was 100°C as is the case for Figures 25–31. Note that the P/P_0 curves do not go through $P/P_0 = 1.0$ at $\lambda = 1.0$, reflecting the effect of heat treatment, which was the same for samples of all draw ratios. Figure 25 shows the same P/P_0 results plotted against film birefringence. The birefringence is a more physically meaningful correlating parameter as it represents a quantitative measure of the actual extent of chain alignment in the polymer as opposed to the draw ratio which is a macroscopic quantity that usually does not describe the microscopic orientation state in the system. The chain orientation function f, which can be defined as the fraction

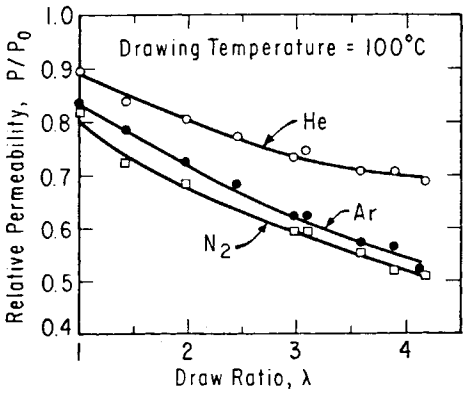

Fig. 24. Permeability, relative to "as-received" value P_0 at 35°C for He, Ar, and N_2 in PVC as a function of draw ratio. (Drawing temperature = 100°C.) P_0 values are tabulated in Table II.

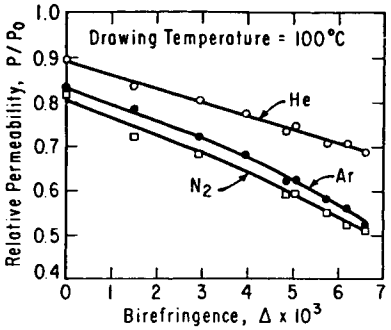

Fig. 25. Relative permeability at 35°C for He, Ar, and N_2 as a function of birefringence. (Drawing temperature = 100°C.)

of polymer segments aligned along the drawing axis, is related to birefringence Δ by

$$f = \Delta/\Delta^0 \tag{4}$$

where Δ^0 is the intrinsic birefringence or the limiting Δ value for the completely oriented material. The intrinsic birefringence can be evaluated theoretically using the polarizabilities of the constituent bonds in the PVC repeating unit. Hibi et al.[30] arrived at a value of 10.4×10^{-3} for the intrinsic birefringence. More recently, Robinson and Bower[31] reported a value of 13.0×10^{-3}, which they deduced from a study utilizing Raman spectroscopy. Based on the latter value, the maximum draw ratio of 4.2 at 100°C attained in this study corresponds to an orientation function of about 0.5.

In Figures 26 and 27, birefringence is again used to correlate the apparent solubility and diffusion coefficients of Ar and N_2 for samples drawn at 100°C. It was not possible to obtain D_a values for He because the time lags were immeasurably small for this gas. Figure 26 demonstrates how k_a is slightly

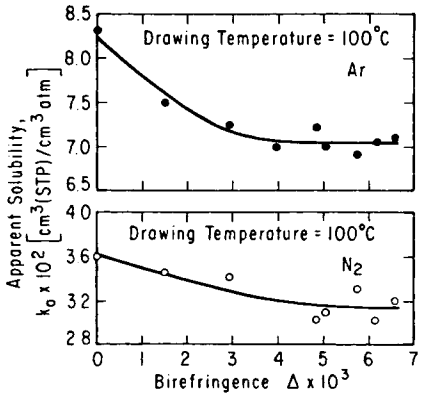

Fig. 26. Apparent solubility for Ar and N_2 in PVC at 35°C vs. film birefringence. (Drawing temperature = 100°C.)

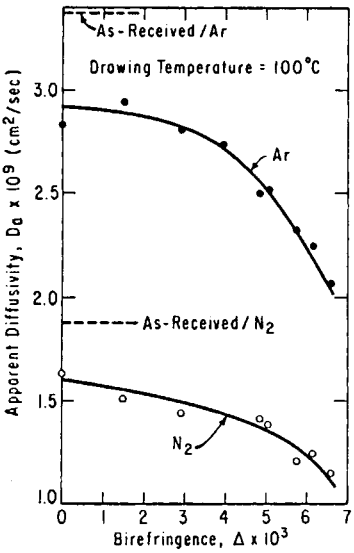

Fig. 27. Apparent diffusion coefficients for Ar and N_2 in PVC at 35°C as a function of film birefringence.

decreased for both Ar and N_2 by orientation. The effect of orientation on the solubility, however, was also dependent on the drawing temperature. This will be dealt with later where the effects of drawing temperature on gas transport are considered.

The response of D_a to orientation is more interesting as seen in Figure 27, where plots for Ar and N_2 against birefringence are shown. For both gases, D_a decreases with Δ and the slopes of the curves become more negative as Δ increases.

Annealing the polymer under strain subsequent to drawing, which causes a slight increase in density as seen in Figure 15, did not produce any significant further reductions in the transport parameters of the oriented film. A sample drawn 3.5X at 100°C and then annealed at this temperature for 15 more minutes had only 5% lower P and D_a values compared to the film not exposed to such post-drawing treatment. By comparing the density and DSC data of oriented specimens with those of the annealed ones, it becomes evident that the transport response to orientation is not related to the same processes governing the annealing behavior analyzed above. Thus, an alternative approach must be considered to explain the observed trends.

Free volume changes cannot be of use for explaining these responses since the density remains essentially constant during drawing, so that the process of gas transport will be considered from the activated state approach in which the diffusion coefficient D, in this case D_a, is given by the well-known Arrhenius expression

$$D = D_0 e^{-E_D/RT} \tag{5}$$

where E_D, the activation energy, is known to be related to the cohesive energy density of the polymer[42] while the preexponential factor D_0 can be

related through Eyring's transition state theory to the activation entropy, which is, in turn, related to the entropic state of the polymer.

Deformation of a rubberlike network, as in the case of drawing above T_g, causes a reduction in the entropy of the network which according to the rubber elasticity theory is proportional to the quantity Γ defined as

$$\Gamma = [\lambda_1^2 + \lambda_2^2 + \lambda_3^2 - 3] \tag{6}$$

where the λ_i are deformation ratios along the three principal axes of the specimen. For uniaxial drawing at constant volume,

$$\lambda_2 = \lambda_3 = \frac{1}{\sqrt{\lambda_1}} = \frac{1}{\sqrt{\lambda}} \tag{7}$$

so that

$$\Gamma = [\lambda^2 + 2/\lambda - 3] \tag{8}$$

If one assumes that this change in entropy of the polymer on drawing translates into a change in the entropy of activation for diffusion, then ln D_0 should be linearly related to Γ. If this physical process of orientation does not change the activation energy E_D, then also ln D should be linearly related to Γ since

$$\ln D = \ln D_0 - E_D/RT \tag{9}$$

Figure 28 shows plots of ln D vs. Γ for Ar and N_2. Interestingly, both sets of data form quite good straight lines (correlation coefficients for Ar and N_2 are -0.996 and -0.957, respectively) with essentially identical slopes.

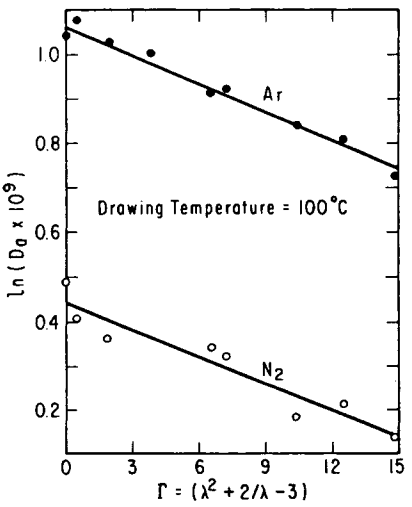

Fig. 28. Apparent diffusion coefficients correlated with the rubber elasticity parameter.

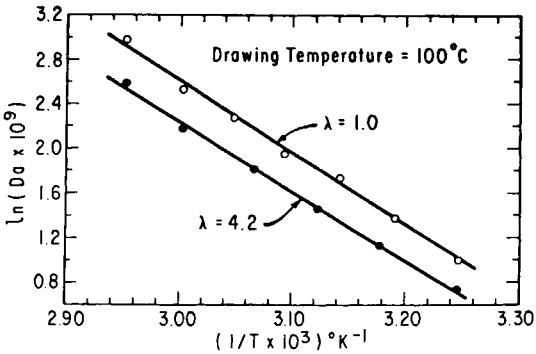

Fig. 29. Apparent diffusion coefficient of Ar for heat-treated (λ = 1.0) and drawn (λ = 4.2) PVC plotted in the Arrhenius form.

To further examine the relative effect of drawing on the parameters D_0 and E_D, the transport of Ar was measured as a function of temperature between the limits of 35 and 65°C. After the series of runs between 35 and 65°C, no measurable loss in birefringence for oriented samples was observed. Figure 29 shows an Arrhenius plot for apparent diffusion coefficients of Ar in PVC for samples with λ = 1.0 and 4.2 prepared at 100°C. Drawing causes a very slight reduction in E_D, but the main effect is a reduction in the preexponential factor, consistent with the arguments outlined above and the results shown in Figure 28. These results differ from the findings of Barker et al.,[6] who report increases in D_0 for poly(alkyl methacrylates). Ito,[32] on the other hand, obtained results similar to ours for CO_2 and polycarbonate.

Figures 30 and 31 present the permeability and apparent solubility coefficients from this series of transient permeation measurements using the Arrhenius form. Orientation causes an increase in both the activation energy E_P and the preexponential factor P_0 for permeation. The net effect is that orientation has a larger effect on the permeability coefficient at low temperatures than at high temperatures. The effect of orientation on the apparent solubility coefficient is even more interesting in that the lines for the drawn and undrawn PVC cross such that the undrawn material has a greater temperature dependence, indicative of a larger apparent heat of solution. However, since k_a is a composite parameter equivalent to $k_D + C'_H b$ in terms of the dual sorption model, the exact meaning of this trend is difficult to interpret without resolving this parameter into its individual

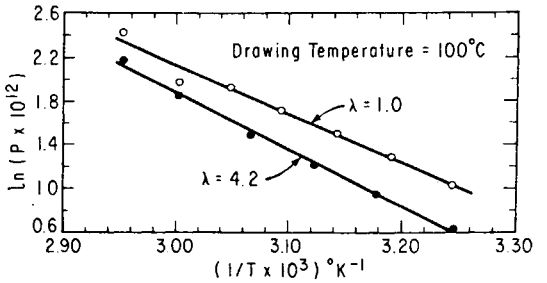

Fig. 30. Ar permeability for heat-treated (λ = 1.0) and drawn (λ = 4.2) PVC plotted in the Arrhenius form.

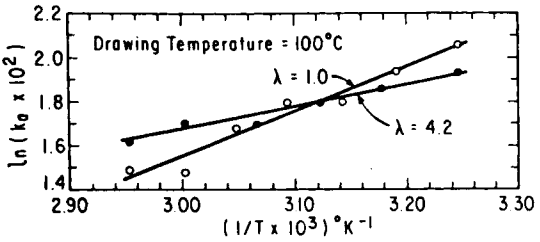

Fig. 31. Apparent solubility of Ar for heat-treated (λ = 1.0) and drawn (λ = 4.2) PVC plotted in the Arrhenius form.

components from detailed analysis of sorption isotherms, which was not done. The parameters deduced from the plots shown in Figures 29–31 for describing the temperature dependence of D_a, k_a, and P are listed in Table V.

Wang and Porter[7] successfully correlated their data on drawn polystyrene using the Cohen and Turnbull free volume model, which can be written as

$$D = A \exp\left[\frac{-\gamma v^*}{\alpha v_m (T - T_0)}\right] \tag{10}$$

where A = empirical preexponential factor, v^* = critical volume required for a penetrant molecule to diffuse, v_m = actual volume of penetrant molecule, γ = an overlap factor (often close to unity), and α = the planar thermal expansivity for the polymer. The anisotropy induced by drawing the polymer results in different linear expansivities along and perpendicular to the draw direction, $\alpha_\parallel$ and $\alpha_\perp$, whose sum is equal to α, so that eq. (10) can be rewritten as

$$D = A \exp\left[\frac{-\gamma v^*}{(\alpha_\parallel + \alpha_\perp) v_m (T - T_0)}\right] \tag{11}$$

Since orientation has been found to reduce the quantity $(\alpha_\parallel + \alpha_\perp)$ relative to its value for the isotropic material, this change is expected to manifest itself as a reduction in D. A plot of ln D against $(\alpha_\parallel + \alpha_\perp)^{-1}$ should thus be also expected to yield a straight line as reported by Wang and Porter. Using

TABLE V
Activation Energies, Preexponential Factors, and Heats of Solution for Ar Transport in Heat-Treated (λ = 1.0) and Drawn (λ = 4.2) PVC

Parameter	Heat-treated at 100°C (λ = 1.0)	Drawn at 100°C (λ = 4.2)
E_p (kcal/mol)	8.879	10.35
P_0 [cm³(STP)cm/cm² s cm Hg]	5.576×10^{-6}	3.982×10^{-5}
E_{Da} (kcal/mol)	12.917	12.40
D_{a0} (cm²/s)	3.998	1.266
ΔH_s (kcal/mol)	−4.028	−2.056
k_{a0} [cm³(STP)/cm³ atm]	1.075×10^{-4}	2.379×10^{-3}

Hellwege's thermal expansivity data for uniaxially oriented PVC,[43] the above procedure was attempted by plotting ln D_a and ln P against $(\alpha_\parallel + \alpha_\perp)^{-1}$. Neither plot, however, yielded the expected linear dependence and both exhibited a strong curvature similar to that of Figure 27. PVC most probably differs from amorphous polystyrene in its degree of internal molecular order. One indication of this is the birefringence response to orientation above T_g in the two polymers. Polystyrene obeys the affine deformation mechanism, illustrated in Figure 32, which is characteristic of rubbers,[7,29] whereas PVC, like polycarbonate,[44] is found to allow a pseudo-affine deformation mechanism, which describes crystallite orientation in many semicrystalline polymers. Another difference is manifested in the dependence of the birefringence on the drawing temperature. As seen in Figure 12, PVC exhibits only about 20% reduction in Δ by drawing at $(T_g + 25)$ relative to the value for drawing at T_g. Over a similar temperature interval Wang and Porter[45] observed over a tenfold reduction in Δ for atactic polystyrene.

Effects of Processing Temperature

The effects of drawing or heat-treatment on gas transport properties depend not only on the extent of orientation but also on the processing temperature employed. To study this temperature dependence, the parameters P, D_a, and k_a for Ar were measured for samples processed at temperatures ranging from 50 to 125°C at draw ratios of 1.0 and 3.0. The sample drawn at 50°C has a draw ratio of 2.8, which was the maximum attainable draw ratio at that temperature. Some data for N_2 followed similar trends to those reported here for Ar. We shall consider the effects of processing temperature on P, D_a, and k_a separately.

The behavior of D_a over the range of processing temperatures (50–125°C) is depicted in Figure 33. The curve for $\lambda = 1.0$ exhibits a minimum in D_a at about 100–110°C. It is interesting that the location of this minimum almost coincides with that of the maximum for the endotherm area shown in Figure 20. In fact, the two trends are essentially mirror images of one another. Thus, the D_a data for annealed PVC correlate better with DSC endotherm data than they do with density. This response of D_a to annealing agrees well with Brady's findings for oxygen.[5] For samples drawn above T_g ($\lambda = 3.0$), D_a follows a similar trend as for the undrawn material. However,

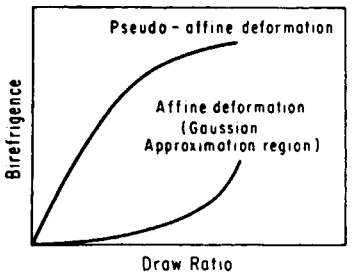

Fig. 32. Birefringence response to uniaxial drawing in two theoretical schemes of deformation. (Figure adapted from Ref. 29.)

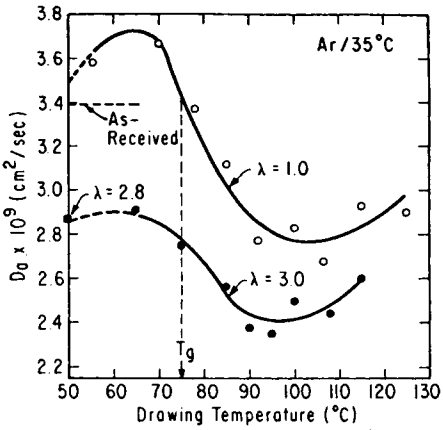

Fig. 33. Apparent diffusion coefficient of Ar in PVC at 35°C vs. processing temperature for annealed (λ = 1.0) and drawn (λ = 3.0) samples.

at high drawing temperatures, the 3X curve is expected to increase more rapidly since the birefringence declines with increasing temperature as shown in Figure 12.

The behavior of D_a for the two samples processed below T_g is quite unexpected. As the treatment temperature is lowered from T_g, D_a increases, reaches a maximum, and then returns to the base value for the as-received film at temperatures below 50°C. The increase in D_a seems consistent with the density data for sub-T_g-annealing shown in Figure 14. However, Illers,[35] for example, reported significant decreases (~30%) in P as a result of annealing just below T_g. The DSC scans of Figure 21 show no features for the 70°C-annealed sample other than the well-known shift in position and height of the sub-T_g relaxation peak. For the sub-T_g drawn samples, D_a is about 15% lower than for the "as-received" material. It must be noted that the annealing time for the sample annealed at 55°C was 36 h instead of the 15 min used uniformly for all other samples. This exception was made considering the slow relaxation rate for the polymer 20°C below its T_g.

The apparent Ar solubility data for annealed and drawn PVC are reported in Figure 34. The effects of processing temperature on k_a result in bell-

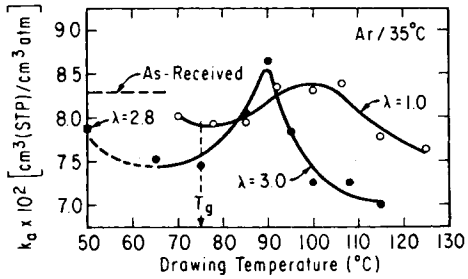

Fig. 34. Apparent solubility of Ar in PVC at 35°C vs. processing temperature for annealed (λ = 1.0) and drawn (λ = 3.0) samples.

shaped curves that have their maxima at 100 and 90°C, for the 1X and 3X samples, respectively. A very similar curve for the k_a of O_2 ws reported by Brady et al.[5] in the case of the annealed samples, but the results for drawn materials cannot be compared since Brady's work was limited to biaxial orientation. The 3X data exhibit a more narrow and pronounced maximum than for the annealed samples.

The maxima in Figure 34 correspond approximately to the minima in D_a seen in Figure 33. The sorption maxima are apparently another manifestation of the temperature dependent "ordering" process indicated by the DSC results shown in Figure 20. As explained earlier, annealing at temperatures above T_g alters the microstructural organization on the molecular or segmental level. The rate of this process is highest at temperatures that are moderately above T_g. At T_g, segmental motions are still somewhat restricted while at temperatures 50°C above T_g vigorous backbone mobility tends to destroy any induced molecular order—a situation somewhat analogous to the interplay of kinetic and thermodynamic factors in crystallization. Since (T_g + 50°C) generally defines the onset of liquidlike backbone mobility in polymers, an annealing temperature of (T_g + 25°C) or 100°C seems reasonable for inducing the highest level of order in PVC. This temperature shifted to 90°C for the oriented samples, presumably because in the oriented state only shorter polymer segments are free to participate in cooperative motions, leading to ordered structures since longer segments are restrained by the segments elongated under strain.

The reasons that the apparent solubility is highest at processing temperatures near 90–100°C appear to stem from the decreased mobility of segments associated with the structural order, which results in greater propensity for intersegmental void regions to serve as gas sorption sites. The gradual loss of this molecular order at processing temperatures above 90–100°C is also evident in Figure 33 from the trend towards increased D_a at higher processing temperatures.

Finally, the effects of processing temperature on the permeability of annealed and drawn PVC to Ar and He are shown in Figure 35. The permeability data reflect the combined effects of mobility and solubility discussed separately above. For annealed samples the permeability decreases essen-

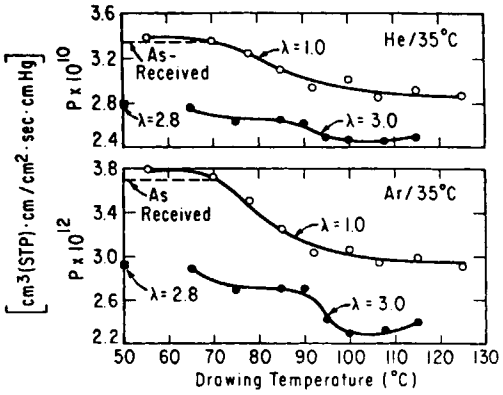

Fig. 35. PVC permeability to He and Ar at 35°C vs. processing temperature for annealed (λ = 1.0) and drawn (λ = 3.0) samples.

tially monotonically, leveling off above about 90°C. Annealing at temperatures above 125°C increases the permeability again according to Brady's study, but such high temperatures were not investigated in this work. For samples drawn at temperatures 90°C or below, the permeabilities are essentially constant. Between 90 and 100°C, P for Ar drops abruptly by 17% owing to the reduction in solubility observed in Figure 34. Beyond 100°C, P increases slightly with higher drawing temperatures. The same trends but to a lesser extent were observed for He.

CONCLUSIONS

Several conclusions can be drawn from the findings of this investigation. The sorption of CO_2 in PVC is much higher than expected on the basis of established correlations and comparisons with other polymers. This is believed to stem from a specific interaction between CO_2 and the PVC repeating unit which increases the amount of CO_2 dissolved by the Henry's law mode since the amount sorbed by the Langmuir mode appears normal. This interaction-specific sorption is believed to be responsible for the extreme plasticizing or conditioning effects observed for CO_2 and PVC. Annealing PVC at temperatures above T_g induces some form of molecular order in the polymer. This order is accompanied by a rise in density and the appearance of endothermic peaks in the DSC thermograms. The highest level of order is achieved by annealing at temperatures around (T_g + 25°C). A minimum in the apparent diffusion coefficient for Ar was observed for this region of annealing temperatures.

Uniaxial drawing has some effect on gas solubility in the polymer, but this depends on the drawing temperature. The effect is most pronounced at drawing temperatures $\sim$(T_g + 25°C). The apparent diffusion and solubility coefficients are dependent on the drawing temperature employed but in different ways. For example, D_a undergoes a *minimum* at processing temperatures of 90–100°C depending on the draw ratio, whereas k_a goes through a *maximum* in the same temperature region.

The permeability and diffusion coefficients decrease with increasing extent of uniaxial molecular orientation in PVC. These reductions are the result of an increased permeation activation energy E_p and a reduced diffusion preexponential factor D_0. The diffusion activation energy E_D remained essentially constant with orientation, but the increase in E_p was brought about by a reduced apparent heat of solution with orientation. Due to these factors, the effectiveness of molecular orientation in improving the barrier character of PVC is best at low temperatures. Finally, while both annealing above T_g and molecular orientation reduce the permeation and diffusion of gases in PVC, they appear to do so via different mechanisms.

This research was sponsored by the National Science Foundation through Grants DMR-80-01665 and CPE-83-06952. Appreciation is expressed to Klockner Pentaplast of America and to Dr. A. R. Berens of B. F. Goodrich for the samples of film provided for this research.

References

1. P. W. Morgan, *Ind. Eng. Chem.*, **45**, 2296 (1943).
2. S. A. Reitlinger and I. S. Yarkho, *Colloid J. (U.S.S.R.)*, **17**, 369 (1955).
3. S. W. Lasoski and W. H. Cobbs, Jr., *J. Polym. Sci.*, **36**, 21 (1959).

4. H. B. Hopfenberg and V. Stannett, in *The Physics of Glassy Polymers,* R. N. Haward, Ed., Elsevier, Amsterdam, 1972, Chap. 9.

5. T. E. Brady, S. A. Jabarin, and G. W. Miller, in *Permeability of Plastic Films and Coatings to Gases, Vapors and Liquids,* H. B. Hopfenberg, Ed., Plenum, New York, 1974, pp. 301–320.

6. R. E. Barker, R. C. Tsai, and R. A. Willency, *J. Polym. Sci., Polym. Symp. Ed.,* **63**, 109 (1978).

7. L. H. Wang and R. S. Porter, *J. Polym. Sci., Polym. Phys. Ed.,* **22**, 1645 (1984).

8. Personal communication with Dr. A. R. Berens of B. F. Goodrich.

9. F. W. Billmeyer, Jr., *Textbook of Polymer Science,* 2nd ed., Wiley-Interscience, New York, 1971, p. 507.

10. W. J. Koros, D. R. Paul, and A. A. Rocha, *J. Polym. Sci., Polym. Phys. Ed.,* **14**, 687 (1976).

11. W. J. Koros and D. R. Paul, *J. Polym. Sci., Polym. Phys. Ed.,* **14**, 1903 (1976).

12. W. J. Koros, D. R. Paul, M. Fujii, H. B. Hopfenberg, and V. Stannett, *J. Appl. Polym. Sci.,* **21**, 2899 (1977).

13. W. J. Koros, A. H. Chan, and D. R. Paul, *J. Membr. Sci.,* **2**, 165 (1977).

14. A. H. Chan and D. R. Paul, *Polym. Eng. Sci.,* **20**, 87 (1980).

15. A. R. Berens, *Polym. Eng. Sci.,* **20**, 95 (1980).

16. B. R. Bird, W. E. Stewart, and E. N. Lightfoot, *Transport Phenomena,* Wiley, New York, 1960, pp. 744–745.

17. K. Toi, G. Morel, and D. R. Paul, *J. Appl. Polym. Sci.,* **27**, 2997 (1982).

18. P. Masi, D. R. Paul, and J. W. Barlow, *J. Polym. Sci., Polym. Phys. Ed.,* **20**, 15 (1982).

19. A. J. Erb and D. R. Paul, *J. Membr. Sci.,* **8**, 11 (1981).

20. W. J. Koros, paper presented at the AIChE Spring Meeting, Anaheim, CA, May 1984.

21. D. R. Paul and W. J. Koros, *J. Polym. Sci., Polym. Phys. Ed.,* **14**, 675 (1976).

22. B. P. Tikhomirov, H. B. Hopfenberg, V. Stannett, and J. L. Williams, *Makromol. Chem.,* **118**, 177 (1968).

23. R. W. Roberts and K. Kammermeyer, *J. Appl. Polym. Sci.,* **7**, 2183 (1963).

24. A. H. Chan and D. R. Paul, *J. Appl. Polym. Sci.,* **24**, 1539 (1979).

25. A. G. Wonders and D. R. Paul, *J. Membr. Sci.,* **5**, 63 (1979).

26. J. S. Chiou, J. W. Barlow, and D. R. Paul, *J. Appl. Polym. Sci.,* to appear.

27. D. Raucher and M. D. Sefcik, in *Industrial Gas Separations,* T. E. Whyte, Jr., C. M. Yon, and E. H. Wagener, Eds., Am. Chem. Soc., Washington, DC, 1983, Chap. 5.

28. S. A. Stern and V. Saxena, *J. Membr. Sci.,* **7**, 47 (1980).

29. L. Holliday and I. M. Ward, in *Structure and Properties of Oriented Polymers,* I. M. Ward, Ed., Applied Science, London, 1975, Chap. 1.

30. S. Hibi, M. Maeda, H. Kubota, and T. Miura, *Polymer,* **18**, 143 (1977).

31. M. E. R. Robinson and D. I. Bower, *J. Polym. Sci., Polym. Phys. Ed.,* **16**, 2115 (1978).

32. Y. Ito, *Kobunshi Kagaku,* **19**, 412 (1962).

33. M. J. El-Hibri, unpublished data.

34. F. P. Reding, E. R. Walter, and F. J. Welch, *J. Polym. Sci.,* **56**, 225 (1962).

35. K.-H. Illers, *Makromol. Chem.,* **127**, 1 (1969).

36. J. A. Juijn, J. H. Gisolf, and W. A. de Jong, *Kolloid Z.,* **235**, 1 (1969).

37. H. R. Brown, G. M. Musindi, and Z. H. Stachurski, *Polymer,* **23**, 1508 (1982).

38. J. L. Koenig and M. K. Antoon, *J. Polym. Sci., Polym. Phys. Ed.,* **15**, 1379 (1977).

39. A. R. Berens and I. M. Hodge, *Macromolecules,* **15**, 756 (1982).

40. T. M. Birshtein and O. B. Ptitsyn, *Conformations of Macromolecules,* Wiley-Interscience, New York, 1966, Chap. 8.

41. M. V. Volkenshtein and O. B. Ptitsyn, *Zh. Tekhn. Fiz.,* **25**, 662 (1955).

42. C. A. Cumins and T. K. Kwei, in *Diffusion in Polymers,* G. Crank and J. S. Park, Eds., Academic, London, 1968.

43. K. H. Hellwege, J. Hennig, and W. Knappe, *Kolloid Z. Z. Polym.,* **188**, 121 (1963).

44. E. Ito, K. Sawamura, and S. Saito, *Colloid Polym. Sci.,* **253**, 480 (1975).

45. L. H. Wang and R. S. Porter, *J. Polym. Sci., Polym. Phys. Ed.,* **21**, 1815 (1983).

Received November 6, 1984
Accepted January 17, 1985